Stark transitions in antiprotonic helium

J. E. Russell
Physics Department, University of Cincinnati, Cincinnati, Ohio 45221-0011
(Received 26 July 2001; revised manuscript received 29 October 2001; published 20 February 2002)

Collisional Stark rates for $\bar{p}^4He^+$ with $36 \lesssim n \lesssim 38$ are estimated with coupled-channel calculations. Both an atomic and a molecular model are used. Matrix elements of the $\bar{p}He^+$-He interaction for the atomic model are approximated with expressions having two or three parameters. Rough estimates for the molecular model are obtained using the generalized Born-Oppenheimer approximation, together with matrix elements for the atomic model. Guesswork, based on interactions of seemingly similar atoms, is used to set fairly wide limits to parameters for the atomic model, it being assumed that the potentials depend only on *n*, *l*, and *R*. Transitions are found to be unlikely. But the rates are sensitive to the potentials. Transitions can be likely if the potentials are different from what can reasonably be guessed by assuming a dependence on only *n*, *l*, and *R*. A potential with a minimum, preferably relatively deep, at relatively small *R* can cause transitions to be important. It is conjectured that this can occur because $\bar{p}He^+$-He potentials depend on the component of $\bar{p}He^+$ intrinsic angular momentum along **R**. Also, it is found that the difference in the reduced mass of $\bar{p}He^+$ and He can cause the rate to be several times higher for $\bar{p}^3He^+$ than for comparable $\bar{p}^4He^+$.

DOI: 10.1103/PhysRevA.65.032509 PACS number(s): 36.10.−k

I. INTRODUCTION

A comparatively low Stark transition rate is necessary if a metastable antiprotonic helium atom ($\bar{p}He^+$) is to undergo a radiative transition [1,2]. By Stark transition we mean a collisionally induced transition of $\bar{p}He^+$ in which its orbital angular momentum *l* changes but its principal quantum number *n* remains the same. By metastable we mean that the Auger rate is, at the very most, not much greater than the radiative rate.

In two experiments in gaseous helium at high densities and at temperatures $T \approx 6$ K, collisionally induced depopulation of the metastable ($n=37, l=34$) state of $\bar{p}^4He^+$, and also of the very similar (36,33) state of $\bar{p}^3He^+$, has been found to be far more probable than for some seemingly less well-shielded states with *n* one or two units higher [3,4]. Also, the depopulation rate for the (36,33) state of $\bar{p}^3He^+$ is approximately ten times larger than for the (37,34) state of $\bar{p}^4He^+$. These experiments have prompted this paper, which presents estimates of Stark rates.

Even without Refs. [3,4], Stark rates would be needed because of other studies of $\bar{p}He^+$ [5]. Largely in accordance with arguments and calculations in Refs. [1,2], some states remain populated until radiation occurs. However, there is some quenching in certain instances. It is dependent on both phase and density [6].

To our knowledge, the only published theoretical investigation of Stark mixing in $\bar{p}He^+$ is a semiclassical calculation by Korenman for states with $n > 42$, where there should be little shielding of the $\bar{p}$ [7]. The present paper describes a quantum mechanical calculation of Stark rates for some lower, presumably much more well-shielded states, including those studied in Refs. [3,4]. We will show that transitions are unlikely in many instances. But due to uncertainties in the $\bar{p}He^+$-He interaction, exceptional cases cannot be ruled out. We will conjecture that such cases occur because the interatomic potential depends on the orientation of the $\bar{p}He^+$ (the component of its intrinsic orbital angular momentum) along the momentary direction of the interatomic separation. The present paper does not account in detail for the experiments, but it defines the Stark problem more precisely.

After much of the work reported here had been completed, we learned of some calculations of diagonal elements of the $\bar{p}He^+$-He interaction, prompted by a different problem, the determination of corrections to the spectrum of $\bar{p}He^+$ due to collisional broadening [8]. These corrections also require interatomic potentials, though for separations somewhat larger than the ones relevant to Stark transitions. The potentials in Ref. [8] were not given in terms of the $\bar{p}He^+$ orientation, as we have defined it. But in some instances a potential was given as a function of two vector separations, one between the $\bar{p}$ and its He^{++} nucleus, the other between the centers of mass of the two atoms. In some other instances it was averaged, for given *n* and *l*, over the former separation and presented as a function of the magnitude of the latter. Some of our calculations take into account some of the results of Ref. [8].

A. Some relevant numbers

For fixed *n*, the energy of $\bar{p}He^+$ decreases with decreasing *l*. Accurate values of the decreases are given by Korobov and Bakalov [9]. The splitting between the (37,34) and (37,33) states of $\bar{p}^4He^+$ is 0.011 265 a.u. All metastable states of $\bar{p}He^+$ are separated from a state with the same *n*, but with *l* one unit lower, by an energy difference of roughly this size. This difference is ~400 times greater than the mean energy of relative motion of $\bar{p}He^+$ and ordinary helium at $T=6$ K. Therefore, *l* decreases in a Stark transition. Also, the probability of a transition in a single collision should ordinarily be small [10]. Because the energy change is always large and always nearly the same, the reduced wavelength of final relative motion is always $\lambda\!\!\!^{-} \sim 0.1$ a.u. But it has a mass dependence. For example, $\lambda\!\!\!^{-}$ is 12% larger for a transition from the (36,33) state of $\bar{p}^3He^+$ than from the otherwise very similar (37,34) state of $\bar{p}^4He^+$. In any event,

λ is smaller than most distances characteristic of the collision. Therefore, the transition rate should depend on the detailed behavior of the $\bar{p}\mathrm{He}^+$-He interaction.

B. Approximating the $\bar{p}\mathrm{He}^+$-He interaction

We will resort to simple approximations. We will also resort to guesswork based on existing studies of interactions between atoms that might appear to be more or less similar to $\bar{p}\mathrm{He}^+$ and He. We will take into account (i) an experimental investigation of the low-energy scattering of atomic hydrogen by noble gases [11,12] and (ii) estimates of interactions of ordinary helium with kaonic helium ($K^-\mathrm{He}^+$) in states with $n=27$, 28, or 29 and $l=n-1$ [13]. We will also keep in mind Ref. [8].

As in the (n,l)-dependent calculations for $\bar{p}\mathrm{He}^+$-He in Ref. [8], the numerical estimates in Ref. [13] of diagonal elements of the $K^-\mathrm{He}^+$-He interaction took no account of any dependence on the orientation of the exotic helium atom. In a sense, neither do any of the approximations to diagonal elements of the $\bar{p}\mathrm{He}^+$-He interaction actually used in computations for the present paper. But we will include a discussion of how such a dependence can arise, and we will keep this possibility in mind when interpreting estimates of Stark rates.

We will consider only states of $\bar{p}\mathrm{He}^+$ comparable to those of $K^-\mathrm{He}^+$ discussed in Ref. [13]. We will approximate the $\bar{p}\mathrm{He}^+$-He interaction with simple, physically reasonable expressions depending on just a few parameters. We will often use Buckingham Exp-6 potentials.

There are two reasons why Exp-6 potentials will be used. Both require van der Waals forces to be taken into account. (i) Rough guesses show that the depth of the van der Waals potential for $\bar{p}\mathrm{He}^+$-He should be at least comparable in magnitude to the initial energy of relative motion, which suggests that the overlap of the wave functions for the initial and the (much more energetic) final state might depend sensitively on the initial potential. (ii) Conceivably, an explanation of Refs. [3,4] would be an enhancement of the Stark rate by a shape resonance due to the centrifugal barrier. This barrier is partly due to van der Waals forces and partly due to the familiar term $L(L+1)/(2\mu R^2)$, where L is the angular momentum of relative atomic motion, and μ and R are the reduced mass and relative separation. We felt it necessary to investigate this possibility because such resonances are important in one of the studies we have relied upon in our guesswork about the $\bar{p}\mathrm{He}^+$-He interaction [11].

C. Outline of paper

Methods of estimating Stark rates will be presented in Sec. II, where there is also a discussion of approximations to $\bar{p}\mathrm{He}^+$-He matrix elements. Numerical results will be presented in Sec. III, where it will be shown that Stark quenching is unlikely unless the actual interatomic potentials—as compared to potentials guessable by assuming a dependence on only n, l, and R—have their minima, preferably relatively deep, at relatively small separations. It will be conjectured in Sec. IV that there is also a significant dependence of the interatomic potentials on the component of $\bar{p}\mathrm{He}^+$ intrinsic orbital angular momentum along the interatomic axis.

Unless stated otherwise, atomic units will be used.

II. METHODS OF CALCULATION

The position of a helium atom in a space-fixed frame with respect to the center of mass of $\bar{p}\mathrm{He}^+$ is denoted by $\mathbf{R}$. A two-state approximation is used for their relative motion. The initial and final states have definite values of L^2 and $L_z=M$.

Approximate Hamiltonians for the relative atomic motion are constructed by using an atomic or a molecular model to take into account the internal motion of $\bar{p}\mathrm{He}^+$. The axis of quantization for this internal motion depends on the model. In the atomic model, it is the z axis of the space-fixed frame. In the molecular model, it is along $\mathbf{R}$.

As explained in Sec. II B 1, we favor the molecular model because it would be more realistic if it were to be implemented precisely. The atomic model is discussed because it is a very convenient introduction to—and it is also very nearly equivalent to—our very approximate implementation of the molecular model.

With both models, the initial and final states of relative atomic motion will be denoted by Ψ_1 and Ψ_2, written as

$$\Psi(\mathbf{R})=\begin{pmatrix}\Psi_1(\mathbf{R})\\ \Psi_2(\mathbf{R})\end{pmatrix}=\frac{1}{R}\begin{pmatrix}\phi_1(R)Y_{L_i,M_i=0}(\hat{\mathbf{R}})\\ \phi_2(R)Y_{L_f,M_f}(\hat{\mathbf{R}})\end{pmatrix}. \quad (1)$$

This depends explicitly only on $\mathbf{R}$, but both approximate Hamiltonians associate Ψ_1 and Ψ_2 implicitly with atomic states of $\bar{p}\mathrm{He}^+$ having intrinsic orbital angular momenta differing by one unit. The atomic model is outlined in Sec. II A, the molecular model in Sec. II B.

A. Atomic model

1. Hamiltonian for relative atomic motion

Atomic wave functions are used for the internal motion of $\bar{p}\mathrm{He}^+$. They describe the relative motion of the $\bar{p}$ with respect to its He^{++} nucleus. There is no explicit description of the electronic structure. But the electronic structure is important in the $\bar{p}\mathrm{He}^+$-He interaction. We will attempt to take this into account by guesswork, and we will attempt to allow ample margin for error.

Ψ is an approximate solution of

$$H_A\Psi=E\Psi, \quad (2)$$

where E is the energy of relative motion in the entrance channel and H_A is

$$H_A=\frac{1}{2\mu}\mathbf{P}\cdot\mathbf{P}+\begin{pmatrix}V_{11}(R) & V_{12}(\mathbf{R})\\ V_{21}(\mathbf{R}) & V_{22}(R)\end{pmatrix}-\begin{pmatrix}0 & 0\\ 0 & \Delta E\end{pmatrix}. \quad (3)$$

In the preceding equation, $\mathbf{P}$ is

$$\mathbf{P}=\frac{1}{i}\nabla\begin{pmatrix}1 & 0\\ 0 & 1\end{pmatrix},$$

and ΔE is the magnitude of the splitting between the initial and final states of $\bar{p}\mathrm{He}^+$. We will guess V.

2. Diagonal elements of V

We assume, tentatively, that V_{11} and V_{22} depend only on n, l, and R. We approximate them with Buckingham Exp-6 potentials, not always with the same numbers.

(a) Exp-6 potential. This is frequently written as

$$\mathcal{V}_B(R)=\frac{\epsilon}{1-\frac{6}{\alpha}}\left[\frac{6}{\alpha}\exp\left(\alpha\left\{1-\frac{R}{R_m}\right\}\right)-\left(\frac{R_m}{R}\right)^6\right].$$

α determines how steeply $\mathcal{V}_B$ increases as R/R_m becomes much smaller (but not too much smaller) than 1. The minimum, at $R=R_m$, is $-\epsilon$. $\mathcal{V}_B$ has a maximum at very small R, below which it decreases rapidly. We always replace $\mathcal{V}_B$ by an infinitely high barrier at $R<2$.

(b) C_6 instead of R_m. We usually specified the van der Waals coefficient C_6 instead of R_m because we felt it necessary to investigate the effect of possible shape resonances. The behavior of the centrifugal barrier is specified more conveniently in terms of C_6. However, in approximating a potential at relatively small separations, C_6 should be thought of as just one of three parameters specifying the effect of dispersion forces of all orders. Its value need not be related to the asymptotic behavior of the actual potential if the Stark rate is insensitive to V_{11} and V_{22} at large R.

(c) Guessing parameter ranges. Fairly wide tentative limits were selected for ϵ, C_6, and α. We used guesswork, based largely on an assumed similarity of a $\bar{p}\mathrm{He}^+$-He potential to potentials between what might seem to be more or less similar pairs of atoms. It was assumed that $\bar{p}\mathrm{He}^+$ is not too different from a hydrogen atom because the mean $\bar{p}$ orbital radius is roughly half that of the electron.

(d) Range of ϵ. We kept in mind an investigation of scattering of hydrogen atoms by noble-gas atoms [11,12]. The depth of the H-He potential—which is very shallow—is 1.69×10^{-5}; that for H-Ne is 6.98×10^{-5}; and those for H-Ar, H-Kr, and H-Xe are progressively larger. We decided to require $10^{-5}\leqslant\epsilon\leqslant10^{-4}$. Our choice of upper limit, which is greater than what might seem reasonable if V_{11} is to be not too different from the H-He potential, was due to a reluctance to assume that the former is as shallow as the latter.

(e) Range of C_6. Even though it turned out that C_6 need not be related to the asymptotic behavior of the actual potential, we did keep in mind calculations of long-range interactions between atoms that might appear to be not vastly different from $\bar{p}\mathrm{He}^+$ and ordinary helium. Chan and Dalgarno found that C_6 is 2.830 for H-He and 1.4714 for He-He [14]. We also kept in mind that $\bar{p}\mathrm{He}^+$ is, in effect, a polar molecule [15–17]. Shimamura has computed the dipole moment $\mathbf{D}$ of $\bar{p}\mathrm{He}^+$ as a function of the separation $\mathbf{r}$ of $\bar{p}$ from its He^{++} nucleus [17]. If $r\approx0.5$, then $\mathbf{D}\approx-0.25\hat{\mathbf{r}}$. An electric dipole of this magnitude, parallel to its separation from an ordinary helium atom, leads to $C_6\approx0.35$. We tentatively assumed that $\mathbf{D}$ would not have an enormous effect in a fully satisfactory calculation of the interatomic potentials. (We will reconsider this in Sec. II B 3.) We decided to require $1\leqslant C_6\leqslant5$. The principal reason for the high upper limit was a belief that Stark transitions are really due to electric fields at relatively small R. The principal reason for the lower limit was the implied value of R_m. We were initially reluctant to allow R_m to be much less than 5. Ultimately, due to lack of agreement with experiment, we will consider lower values of C_6.

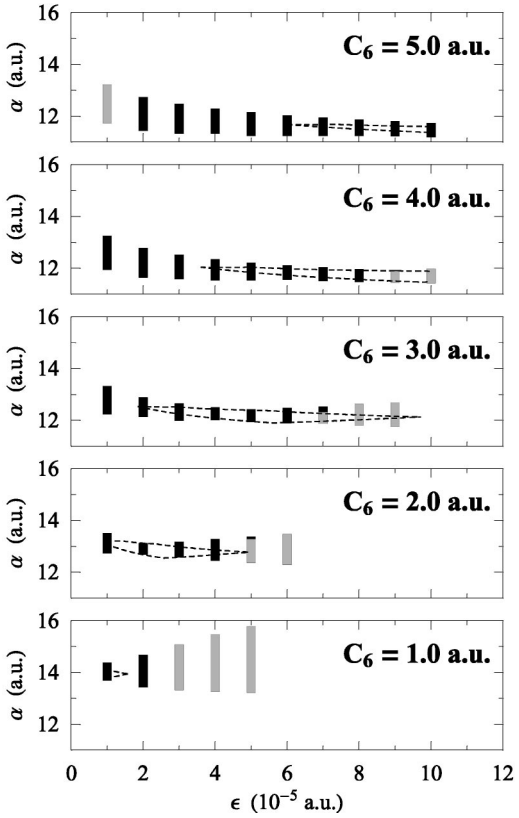

FIG. 1. Vertical bars, in black or gray or both, show the ranges of α. Ranges in gray lead to R_m differing from 6.6 a.u. by more than 20%. Dashed lines enclose all α leading to Exp-6 potentials differing by less than 20% from estimates of a $K^-\mathrm{He}^+$-He potential at $R=2.0$, 2.5, and 3.0 a.u.

(f) Ranges of α. Fairly wide ranges were assigned to α. For given C_6 and ϵ, the range was established by requiring, for $2\leqslant R\leqslant3$, an agreement—of sorts—between V_{11} and the $K^-\mathrm{He}^+$-He potential for $K^-\mathrm{He}^+$ with $n=28$ and $l=n-1$. We attempted to determine two values of α, each leading to equality of these two potentials at $R=2$ or 3. These values specified the allowed range. This *ad hoc* procedure should be acceptable because our Stark rates turn out to be insensitive to variations in α generally wider than the selected ranges, provided $V_{11}=V_{22}$.

(g) Summary of ranges. Figure 1 shows, for $10^{-5}\leqslant\epsilon\leqslant10^{-4}$ and $1\leqslant C_6\leqslant5$, the allowed ranges of α. Figure 1 also shows the usually much narrower ranges of α leading to agreement, to within 20%, of an Exp-6 potential with the $K^-\mathrm{He}^+$-He potential at $R=2.0$, 2.5, and 3.0. This is why we

assert that fairly wide ranges have been selected.

(h) Range of R_m. Our values of ϵ, C_6, and α lead to $4.7 \leqslant R_m \leqslant 8.1$. This is a very wide range. The minima of the potentials between atomic hydrogen and noble-gas atoms are at separations differing from 6.6 by less than $\sim 10\%$ [11,12]. The minima of the (n,l)-dependent $\overline{p}\mathrm{He}^+$-He potentials estimated in Ref. [8] are at $R \approx 5.5$. Figure 1 identifies the combinations of C_6, ϵ, and α causing R_m to differ from 6.6 by more than 20%.

(i) Ranges of n. Our Stark rates were obtained using many combinations of C_6, ϵ, and α, without assigning specific combinations to specific n and l. Even though we established our limits on α by using only estimates for $K^-\mathrm{He}^+$ with $n=28$, many of the potentials obtainable with our allowed parameter combinations should be associable with one or another of several states of $\overline{p}\mathrm{He}^+$, since the $K^-\mathrm{He}^+$-He potentials with $n=27$, 28, and 29 in Ref. [13] are scarcely different from one another. This range for $K^-\mathrm{He}^+$ corresponds to $\overline{p}^3\mathrm{He}^+$ with $35 \leqslant n \leqslant 37$ and $\overline{p}^4\mathrm{He}^+$ with $36 \leqslant n \leqslant 38$.

(j) Typical potential. Some of our rate calculations were performed using

$$C_6 = 2.5, \quad \epsilon = 5 \times 10^{-5}, \quad \alpha = 12.5. \tag{4}$$

This gives a typical potential, in fair agreement with ones determined for $K^-\mathrm{He}^+$-He.

3. Off-diagonal elements of V, and the radial equation

To approximate V_{12}, we guessed an electric field $\mathcal{E}(R)\hat{\mathbf{R}}$ that can be thought of as causing the transition. It was assumed to depend on $\mathbf{R}$, but it was also assumed to be constant for all $\mathbf{r}$. Since the orbital radius of the $\overline{p}$ is ~ 0.5—which is not small compared to the range of R over which V_{11} becomes highly repulsive—$\mathcal{E}(R)$ can be thought of as a R-dependent average field strength unlikely to be related to V_{11} and V_{22} in a simple way.

(a) Perturbing interaction. V_{21} was equated to the matrix element of

$$H' = f\mathcal{E}(R)\hat{\mathbf{R}} \cdot \mathbf{r}, \tag{5}$$

calculated with space-fixed atomic wave functions $\psi_1(\mathbf{r})$ and $\psi_2(\mathbf{r})$ for the initial and final states of $\overline{p}\mathrm{He}^+$. Here, $\mathbf{r}$ is the position of the $\overline{p}$ with respect to its He^{++} nucleus, and f, which is 1.25 for ^{3}He and 1.20 for ^{4}He, takes into account the difference in magnitude of the charges of the $\overline{p}$ and its nucleus, together with the relative position of their center of mass. $\psi_1(\mathbf{r})$ and $\psi_2(\mathbf{r})$ were approximated with hydrogenic functions, both eigenfunctions of

$$H_{\overline{p}}^0 = -\frac{1}{2\mu_{\overline{p}}}\boldsymbol{\nabla}^2 - \frac{Z_{\mathrm{eff}}}{r}, \tag{6}$$

where $\mu_{\overline{p}}$ is the reduced mass of $\overline{p}$ and He^{++}. The quantum numbers of ψ_1 and ψ_2 are (n,l,m_i) and $(n,l-1,m_f)$. Since ΔE was taken into account in Eq. (3), the effective nuclear charge Z_{eff} was assumed to have no l dependence. It was assigned the value obtained by Shimamura for a circular orbit [17]. For $\overline{p}^4\mathrm{He}^+$ with $n=37$, it is $Z_{\mathrm{eff}}=1.797$.

(b) Radial equation. The expressions for V_{12} and V_{21} are inserted in Eq. (3). The two sides of Eq. (2) do not have the same angular dependence. We retain only that part of $H_A\Psi$ having the same angular dependence as Ψ in Eq. (1). This is justified if the cross section is small, which is always the case except near a shape resonance. We must have $L_f = L_i + 1$ or $L_f = L_i - 1$ and $M_f = -1$, 0, or $+1$. The equation coupling ϕ_1 and ϕ_2 is

$$-\frac{1}{2\mu}\frac{d^2}{dR^2}\begin{pmatrix}\phi_1\\ \phi_2\end{pmatrix} + \mathcal{U}_A\begin{pmatrix}\phi_1\\ \phi_2\end{pmatrix} = E\begin{pmatrix}\phi_1\\ \phi_2\end{pmatrix}, \tag{7}$$

where

$$\mathcal{U}_A(R) = \begin{pmatrix}\mathcal{V}_{11}(R) & \mathcal{V}_{12}(R)\\ \mathcal{V}_{21}(R) & \mathcal{V}_{22}(R)\end{pmatrix} - \begin{pmatrix}0 & 0\\ 0 & \Delta E\end{pmatrix}.$$

The diagonal elements of $\mathcal{V}$ are

$$\mathcal{V}_{11}(R) = \frac{L_i(L_i+1)}{2\mu R^2} + V_{11}(R),$$

$$\mathcal{V}_{22}(R) = \frac{L_f(L_f+1)}{2\mu R^2} + V_{22}(R).$$

The off-diagonal elements, containing Clebsch-Gordan coefficients and the radial matrix element $\langle r \rangle_{21}$ of the $\overline{p}$, are

$$\mathcal{V}_{12}(R) = \mathcal{V}_{21}(R) = f\beta_A\mathcal{E}(R)\langle r\rangle_{21}, \tag{8}$$

where

$$\beta_A = \delta_{M_f, m_i - m_f}(-1)^{m_i - m_f + 1}\sqrt{\frac{2L_i+1}{2L_f+1}\frac{l}{2l-1}} \times \langle L_i 1; 00 | L_i 1; L_f 0\rangle \langle L_i 1; 0 m_i - m_f | L_i 1; L_f m_i - m_f\rangle \times \langle l1; m_i m_f - m_i | l1; l-1 m_f\rangle.$$

(c) Guessing $\mathcal{E}(R)$. Because some uncertainty attends the guessing of $\mathcal{E}$, two forms will be used. One form is

$$\mathcal{E}_{\mathrm{exp}}(R) = \mathcal{E}_0 e^{-\eta(R-2.0)}. \tag{9}$$

Choosing

$$\mathcal{E}_0 = 2.29 \times 10^{-2}, \quad \eta = 2.5 \tag{10}$$

gives good agreement, not only at small R but even at R as large as 5. The other form is given in terms of an Exp-6 potential by

$$\mathcal{E}_{\mathrm{E6}}(R) = -\frac{d\mathcal{V}_B}{dR}. \tag{11}$$

Because the orbital radius of the $\overline{p}$ is not negligibly small, the parameters for $\mathcal{V}_B$ in Eq. (11) can be rather different from

those for either of the diagonal elements. They will be denoted by $\epsilon^{(\mathrm{od})}$, $C_6^{(\mathrm{od})}$, and $\alpha^{(\mathrm{od})}$. Choosing

$$\epsilon^{(\mathrm{od})}=5.0\times10^{-5},\quad C_6^{(\mathrm{od})}=0.7,\quad \alpha^{(\mathrm{od})}=10.9 \tag{12}$$

gives fair agreement at small R.

4. Thermally averaged rate

ϕ_2/R is required to have the logarithmic derivative of an outgoing spherical wave at very large R, and ϕ_1/R is decomposed into an incoming and an outgoing wave. The partial cross section is then computed. The cross section $\sigma(E)$ is found by summing partial cross sections over appropriate combinations of L_i, L_f, M_f, and m_f and averaging over m_i.

A Boltzmann distribution was assumed for energies of relative motion between the two atoms. If the number density N of helium atoms does not exceed 10^{21} cm^{-3}, this should be justified because the thermal wavelength $\lambda_T \sim 0.5\times10^{-7}$ cm at $T=6$ K is smaller than the interatomic spacing. This condition is satisfied at the lower pressures employed in Refs. [3,4]. The Stark rate is

$$\gamma_S=N\int_0^\infty \sqrt{2\mu E}\,\sigma(E)f(E)dE, \tag{13}$$

where

$$f(E)=\frac{2}{\sqrt{\pi}}\frac{1}{kT}\sqrt{\frac{E}{kT}}\exp\left(-\frac{E}{kT}\right).$$

B. Molecular model

1. Hamiltonian for relative atomic motion

The $\bar{p}$ is treated more or less as an electron is treated in a diatomic molecule. We use molecular type functions $\psi_1(\mathbf{R},\mathbf{r})$ and $\psi_2(\mathbf{R},\mathbf{r})$ depending adiabatically on $\mathbf{R}$. The Hamiltonian will be invariant with respect to rotations around $\mathbf{R}$. Therefore, ψ_1 and ψ_2 have the same component $m=m_i=m_f$ of the $\bar{p}\mathrm{He}^+$ intrinsic orbital angular momentum along $\mathbf{R}$.

The molecular model, if it were to be precisely implemented, should be better than the atomic model because of the relative speeds of the particles, as computed using classical mechanics. In the initial state, the rms speed of relative motion between $\bar{p}\mathrm{He}^+$ and ordinary helium at $T=6$ K is 2.6×10^4 cm/s for ^{4}He. This is small compared to the similarly calculated speeds of the electrons, and also to that of the $\bar{p}$, which is $\sim1.0\times10^7$ cm/s. The final state is not crucially different. The relative speed of the two atoms, though ~20 times larger than initially, remains much slower than the $\bar{p}$ speed.

The wave function for relative atomic motion is again written as $\Psi(\mathbf{R})$. The Hamiltonian is

$$H_M=\frac{1}{2\mu}[\mathbf{P}-\mathbf{A}(\mathbf{R})]\cdot[\mathbf{P}-\mathbf{A}(\mathbf{R})]+U_M(R). \tag{14}$$

H_M comes from the generalized Born-Oppenheimer approximation [18,19]. It contains a vector potential $\mathbf{A}$ and a scalar potential U_M.

2. Vector potential

Matrix elements of $\mathbf{A}$ are approximated with

$$\mathbf{A}_{jk}=\mathbf{A}_{kj}^*=i\int d^3\mathbf{r}\,\psi_j^*(\mathbf{R},\mathbf{r})\nabla_{\mathbf{R}}\psi_k(\mathbf{R},\mathbf{r}), \tag{15}$$

where $\nabla_{\mathbf{R}}$ is with respect to $\mathbf{R}$. In a precise calculation, the wave functions in Eq. (15) would depend also on the three electrons, they would be exact wave functions for fixed $\mathbf{R}$, and the integration would extend also over the electronic coordinates. Because the electronic structure probably changes very little during a transition, we use functions depending only on $\mathbf{R}$ and $\mathbf{r}$. They are approximate eigenfunctions ψ_i of

$$H_{\bar{p}}=H_{\bar{p}}^0-\Delta E\,\delta_{i,2}+H',\quad i=1,2,$$

where $H_{\bar{p}}^0$ and H' are defined in Eqs. (6) and (5). These functions are written in terms of two eigenfunctions of $H_{\bar{p}}^0$, the latter eigenfunctions being quantized along $\mathbf{R}$ with quantum numbers (n,l,m) and $(n,l-1,m)$. The approximate eigenvalues of $H_{\bar{p}}$ are

$$-\frac{Z^2}{2\mu_p n^2}\pm\frac{\Delta E}{2}(\sqrt{1+t^2}\mp1), \tag{16}$$

where

$$t(R)=\frac{\langle n,l-1,m|H'|n,l,m\rangle}{\frac{1}{2}\Delta E}, \tag{17a}$$

$$\langle n,l-1,m|H'|n,l,m\rangle=f\beta_M\mathcal{E}(R)\langle r\rangle_{21}. \tag{17b}$$

The factor f, the field strength $\mathcal{E}$, and the radial matrix element $\langle r\rangle_{21}$ in Eq. (17b) are the same as in Eq. (8). The factor β_M is

$$\beta_M=\sqrt{\frac{(l-m)(l+m)}{(2l-1)(2l+1)}}\approx\frac{1}{2}\sin\theta_p, \tag{18}$$

where θ_p is the angle between $\mathbf{R}$ and the normal to the plane of a classically described $\bar{p}$ orbit.

3. Scalar potential

The scalar potential is written as

$$U_M(R)=\begin{pmatrix}W_{11}(R)&0\\0&W_{22}(R)\end{pmatrix}-\begin{pmatrix}0&0\\0&\Delta E\end{pmatrix}. \tag{19}$$

In a precise calculation, W_{11} and W_{22} would be the interatomic potentials for the initial and final states, as obtained by equating them to differences between energy eigenvalues of exact wave functions for $\bar{p}$ and electronic motion with fixed R and similarly defined eigenvalues with very large R. They would depend on the component of $\bar{p}$ and electronic orbital angular momentum along $\mathbf{R}$, which we continue to

denote by m. Besides varying adiabatically with $\mathbf{R}$, the electronic motion would vary almost adiabatically with $\mathbf{r}$ [15–17].

(a) Potentials used in computations. We used a sweeping approximation for W_{11} and $W_{22}-\Delta E$,

$$W_{11}=V_{11}+\frac{\Delta E}{2}(-1+\sqrt{1+t^2}), \tag{20a}$$

$$W_{22}-\Delta E=V_{22}+\frac{\Delta E}{2}(-1-\sqrt{1+t^2}). \tag{20b}$$

These expressions were obtained by diagonalizing

$$\begin{pmatrix} V_{11}(R) & f\beta_M\mathcal{E}(R)\langle r\rangle_{12} \\ f\beta_M\mathcal{E}(R)\langle r\rangle_{12} & V_{22}(R)-\Delta E \end{pmatrix}.$$

Unless $V_{11}=V_{22}$, they are not what are obtained in the exact diagonalization of this matrix; but they are convenient in a long computation, and they are accurate enough if

$$|V_{11}(R)-V_{22}(R)|\ll\Delta E,$$

which is a condition that should also be satisfied if ΔE for an isolated $\overline{p}\mathrm{He}^+$ is to be used. W_{11} and W_{22} in Eq. (20) are scarcely different from V_{11} and V_{22} unless R is very small. When interpreting numerical results, we will bear in mind that a better approximation to U_M might have a pronounced m dependence due to a distortion of the electronic wave functions, not taken into account in determining V_{11} and V_{22}.

(b) Possible two-step Born-Oppenheimer calculation. A better approximation to U_M could be found by performing two traditional Born-Oppenheimer calculations, first to determine the electronic motion for fixed $\mathbf{R}$ and $\mathbf{r}$, and second, to determine the $\overline{p}$ motion for fixed $\mathbf{R}$. This should not have much effect on the vector potential. Since only the lowest-lying electronic state would have been taken into account for each combination of $\mathbf{R}$ and $\mathbf{r}$, there would still be no contribution to $\mathbf{A}$ from the electronic motion, as the electronic wave function, which must be normalized for each $\mathbf{R}$, should have constant phase. But the $\mathbf{r}$-dependent distortion of the electronic wave function should have an appreciable effect on U_M. Since calculations presented in Sec. III will show that Stark rates are very sensitive to W_{11}, we add a few more remarks.

(c) Special case: $|m|=l$. We note some general features of W_{11} that can be expected in the especially simple (though not entirely realistic) case $|m|=l$. As before, l denotes the initial $\overline{p}$ orbital angular momentum in the limit of very large R. [Because transitions with $\Delta l=-1$ do not occur in the molecular model from states with $|m|=l$, it would have been more realistic, though more complicated, to consider states with $|m|$ large, but not so large as to cause the angular factor β_M in Eqs. (17b) and (18) to be negligibly small.] Since l is large in metastable $\overline{p}\mathrm{He}^+$, the $\overline{p}$ probability density would be non-negligible only in some region near a plane perpendicular to $\mathbf{R}$ and containing the $\overline{p}\mathrm{He}^+$ center of mass. The $\mathbf{r}$-dependent dipole moment $\mathbf{D}_e$ of the electron charge distribution in $\overline{p}\mathrm{He}^+$, determined with respect to its He^{++} nucleus, is a convenient indicator of the $\mathbf{r}$-dependent distortion of the electron motion. $\mathbf{D}_e$ should almost always be nearly orthogonal to $\mathbf{R}$. This should affect W_{11}. There is an indication of this in Ref. [8], where a $(\mathbf{R},\mathbf{r})$-dependent potential, presented for $r=0.65$ and $R\geqslant 4$, becomes noticeably deeper if $\mathbf{r}$ and $\mathbf{R}$ are nearly orthogonal. In the even more special case $|m|=l$ and $l=n-1$, where the $\overline{p}$ probability density would be confined to a toroidal volume encircling the $\overline{p}\mathrm{He}^+$ center of mass and having a small cross-sectional area, the m-dependent potential that we have in mind should be nearly identical to a potential of the type computed in Ref. [8], provided $\mathbf{r}\cdot\mathbf{R}=0$. The depth of W_{11} for such a state seems likely to be comparatively large if the mean orbital radius of the $\overline{p}$ is nearly equal to the separation for which D_e is greatest. D_e has a broad maximum centered at $r\approx 0.45$ [17].

(d) Probable constraint on l dependence of W_{11}. The detailed form of the m-dependent potential that we have in mind should depend on l as well as n, since it could be approximated, using a two-step Born-Oppenheimer calculation, in terms of energy eigenvalues of an approximate $\overline{p}$ wave function. If coupled-channel calculations are ever to fully account for the results of Refs. [3,4], it would very likely be necessary, for fixed n and $|m|=l$, that the minimum of W_{11} occur at a separation that decreases with decreasing l.

4. Radial equation

No matter what functional form is used for U_M, the equation

$$H_M\Psi=E\Psi \tag{21}$$

must be solved. We retain only the radial part of $\mathbf{A}$ in the expression for H_M given by Eq. (14). This is justified because the initial and final $\overline{p}$ wave functions must have the same azimuthal quantum number m, which allows the integration volume for Eq. (15) to be sorted into pairs of points for which the components of $\psi_j^*\boldsymbol{\nabla}_{\mathbf{R}}\psi_k$ orthogonal to $\mathbf{R}$ have opposite sign. Because $\mathbf{A}$ has no component orthogonal to $\mathbf{R}$, its diagonal elements vanish, and its off-diagonal elements are purely imaginary. $\mathbf{A}$ is written as

$$\mathbf{A}(R)=iB(R)\hat{\mathbf{R}},\quad B(R)=b(R)\begin{pmatrix} 0 & -1 \\ 1 & 0 \end{pmatrix}.$$

The function $b(R)$, as found using our approximate eigenfunctions of $H_{\overline{p}}$, can be written as

$$b(R)=\frac{1}{2}\frac{ds}{dR}\sum_{n=0}^{\infty}(-1)^n s^{2n},$$

where

$$s(R)=t(R)\quad\text{if}\quad|t|<1,\quad s(R)=\frac{1}{t(R)}\quad\text{if}\quad|t|>1.$$

The radial equation is

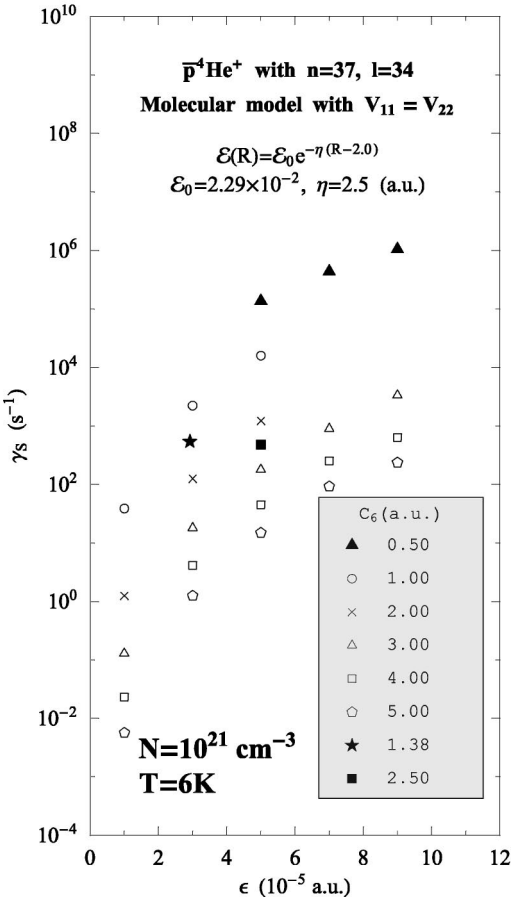

FIG. 2. γ_S for a wide selection of C_6 and ϵ.

$$-\frac{1}{2\mu}\left(\frac{d}{dR}+B\right)^2\begin{pmatrix}\phi_1\\ \phi_2\end{pmatrix}+\mathcal{U}_M\begin{pmatrix}\phi_1\\ \phi_2\end{pmatrix}=E\begin{pmatrix}\phi_1\\ \phi_2\end{pmatrix}, \qquad (22)$$

where

$$\mathcal{U}_M(R)=\begin{pmatrix}\mathcal{W}_{11}(R) & 0\\ 0 & \mathcal{W}_{22}(R)\end{pmatrix}-\begin{pmatrix}0 & 0\\ 0 & \Delta E\end{pmatrix},$$

$$\mathcal{W}_{11}(R)=\frac{L_i(L_i+1)}{2\mu R^2}+W_{11}(R),$$

$$\mathcal{W}_{22}(R)=\frac{L_i(L_i+1)}{2\mu R^2}+W_{22}(R).$$

Equation (22) is different from Eq. (7), but the boundary condition on ϕ_2/R at very large R is the same.

5. Thermally averaged rate

The calculation of transition rates proceeds almost as for the atomic model. The chief difference is that, even though there is a change in the $\bar{p}He^+$ intrinsic orbital angular momentum, the quasiclassical nature of the Born-Oppenheimer approximation results in there being no change in L or M. Also, there is no change in the component of $\bar{p}He^+$ intrinsic orbital angular momentum along **R**.

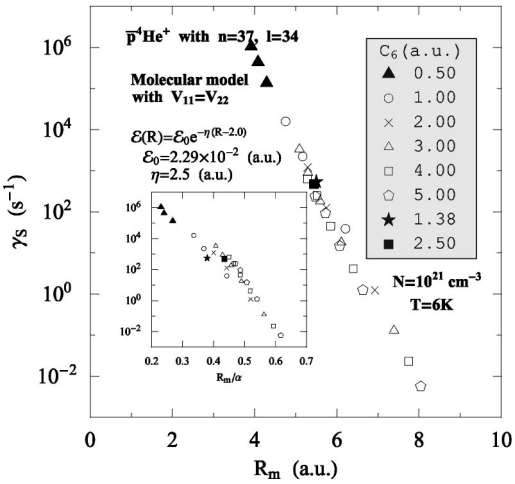

FIG. 3. γ_S with respect to R_m and R_m/α.

III. NUMERICAL RESULTS

A. Introductory remarks

1. Radiative rate, T, L_i, N, and required γ_S

If Stark transitions are to be important, γ_S must be at least comparable to the radiative rate. Most calculated radiative rates of the (37,34) state of $\bar{p}^4He^+$ and the (36,33) state of $\bar{p}^3He^+$ are not very different from one another [16,17,20]. Very roughly, they are $\sim 0.8\times10^6$ s^{-1}.

It was assumed in all computations of γ_S that $T=6$ K.

All computations of γ_S took into account all $L_i \leqslant 5$. Higher L_i are unimportant at $T=6$ K.

It was always assumed that $N=10^{21}$ cm^{-3}.

As reported in Ref. [3], the disappearance rate of the (37,34) state of $\bar{p}^4He^+$ rises almost linearly at almost constant temperature $T\approx6.3$ K from 0.8×10^6 s^{-1} at $N=0.12\times10^{21}$ cm^{-3} to 1.34×10^6 s^{-1} at $N=0.90\times10^{21}$ cm^{-3}. It is necessary to obtain $\gamma_S\approx0.7\times10^6$ s^{-1}.

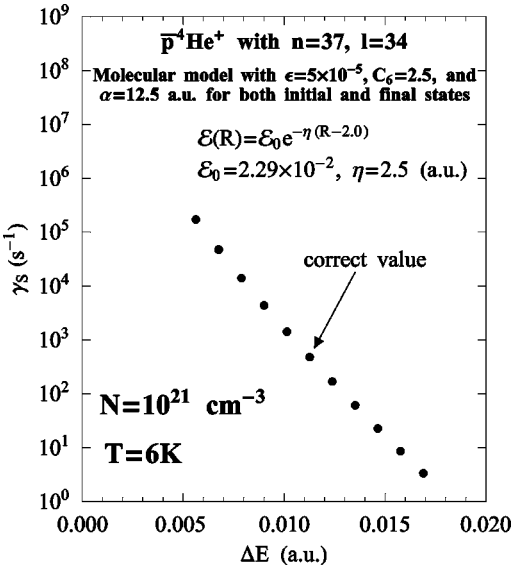

FIG. 4. Typical dependence of γ_S on ΔE.

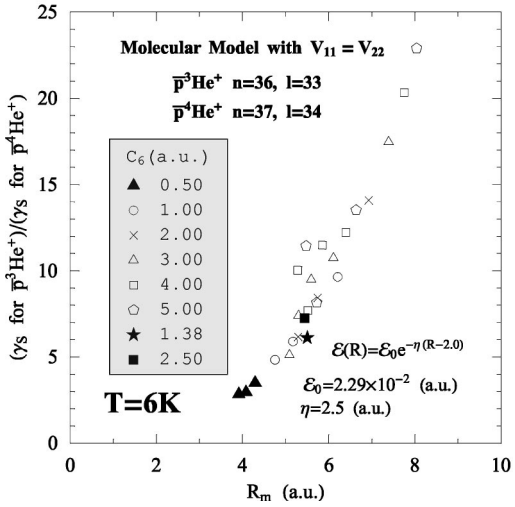

FIG. 5. Ratio of γ_S for $\bar{p}^3\mathrm{He}^+$ to γ_S for $\bar{p}^4\mathrm{He}^+$.

2. Choices of model and input

Most of our results will be presented in Figs. 2–6. The molecular model was used for Figs. 2–5 and a number of other results. The atomic model was used for Fig. 6 and a few other results.

For every figure, $\mathcal{E}$ had the general form $\mathcal{E}_{\mathrm{exp}}$, with the parameters given in Eq. (10). Some calculations using other parameters for $\mathcal{E}_{\mathrm{exp}}$, as well as some calculations using the form $\mathcal{E}_{\mathrm{E6}}$, will be summarized in Sec. III B 3.

Except for a few special instances, most rate estimates were computed using some unchanging input appropriate for the (37,34) state of $\bar{p}^4\mathrm{He}^+$. These data should also be more or less acceptable for nearby states. This input—used to obtain all results in Figs. 2, 3, and 6—comprised values of ΔE, μ, $\mu_{\bar{p}}$, f, l, and $\langle r\rangle_{21}$. Besides Fig. 4, the only instances where these data were different were a few other computations, used for Fig. 5, in which the input was for the (36,33) state of $\bar{p}^3\mathrm{He}^+$.

The unchanging data for $\bar{p}^4\mathrm{He}^+$ did not include parameters for the $\bar{p}\mathrm{He}^+$-He interaction. It was assumed, tentatively, that varying them within their selected ranges would lead to Stark rates that include those for $\bar{p}^4\mathrm{He}^+$ with $36 \lesssim n \lesssim 38$ and $\bar{p}^3\mathrm{He}^+$ with $35 \lesssim n \lesssim 37$.

3. Approximating the sum and average over m_f and m_i

In a precise implementation of the molecular model, in which W_{11} and W_{22} would depend on $m = m_i = m_f$, summing and averaging over m_f and m_i would be very time consuming. Moreover, as will be explained in Sec. III B 3, even a precise implementation of the atomic model would be very time consuming if $\mathcal{E}$ for some values of R were to be stronger than our usual estimates by little more than a factor of 2. But in the actual computations performed with either model, a significant dependence on m_i and m_f occurred only in the factors β_A or β_M in the functions $\mathcal{V}_{12}(R) = \mathcal{V}_{21}(R)$ or $t(R)$ specified by Eqs. (8) or (17). It happens that with both models, and for all choices of $\mathcal{E}_{\mathrm{exp}}$ and $\mathcal{E}_{\mathrm{E6}}$ compatible with the parameter ranges chosen in Sec. II A 3, the estimated Stark rate for given L_i and L_f—averaged thermally, but not summed and averaged over m_f and m_i—varies with β_A or β_M more or less quadratically, in many instances almost precisely so. This permitted γ_S to be estimated by first computing a thermally averaged rate for given L_i and L_f and just one value of β_A or β_M, and then multiplying it by a factor determined from a sum and average of β_A^2 or β_M^2. All estimates of γ_S—even those obtained with what we believe to be unrealistically large $\mathcal{E}$, and for which this procedure turned out to be unjustified—were computed in this way. Some calculations outlined in Sec. III B 3 indicate that the breakdown of the quadratic approximation for large $\mathcal{E}$ does not change any conclusion of the present paper.

4. Purposes of the various calculations

Our principal results will be presented in Figs. 2 and 3, which will show γ_S for wide selections of C_6, R_m, and ϵ. Figures 4–6, and also brief summaries of other results, will be presented for several reasons. (i) To establish that most of the rates in Figs. 2 and 3, as compared to the radiative rate, do not change meaningfully if any of the other parameters for the $\bar{p}\mathrm{He}^+$-He interaction are changed by reasonable amounts. (ii) To relate rates for $\bar{p}^3\mathrm{He}^+$ to those in Fig. 3. (iii) To account for the very wide range of rates in Fig. 3. (iv) To investigate the effect of possible shape resonances. (v) To support a conjecture that an accurate calculation would require W_{11} to depend significantly on the orientation of $\bar{p}\mathrm{He}^+$.

B. Molecular model with $V_{11} = V_{22}$

1. γ_S for $\bar{p}^4He^+$

Figure 2 shows γ_S for 26 parameter sets. These include 21 representative sets from Fig. 1. Four of the other five comprise three sets with $C_6 = 0.5$ and one specified by Eq. (4). The remaining set is

$$C_6 = 1.38, \quad \epsilon = 2.92\times10^{-5}, \quad \alpha = 14.5, \tag{23}$$

which appears to give an acceptable fit to the $\bar{p}\mathrm{He}^+$-He potential presented in Ref. [8] for the (38,34) state of $\bar{p}^4\mathrm{He}^+$. We assume that this set is also appropriate for the (37,34) state. If, as we have also been assuming, V_{11} and V_{22} depend only on n, l, and R, this should be the most realistic set. The rates in Fig. 2, which span eight orders of magnitude, are identified by C_6 and ϵ.

Figure 3 shows the rates in Fig. 2 plotted with respect to R_m and R_m/α. The correlation with R_m is striking, even stronger than with R_m/α.

(a) Values of α. These are not shown in Figs. 2 and 3. They are all between 11.63 and 17.0. They were not all selected in the same way. For $C_6 = 0.5$, 1.0, or 2.0, the value of α is the one that maximizes γ_S. For $C_6 = 3.0$, 4.0, or 5.0, it is either the upper or the lower limit of the allowed range in Fig. 1, whichever gives the larger γ_S. Except if $C_6 = 0.5$ or 1.38, it is between 11.63 and 14.15. The rates for $C_6 = 0.5$ have $\alpha = 16.0$ or 17.0. Not always choosing α in the same way has little effect on γ_S.

(b) Comparison with experiment. None of the rates in Figs. 2 and 3 for parameters within our selected ranges is compat-

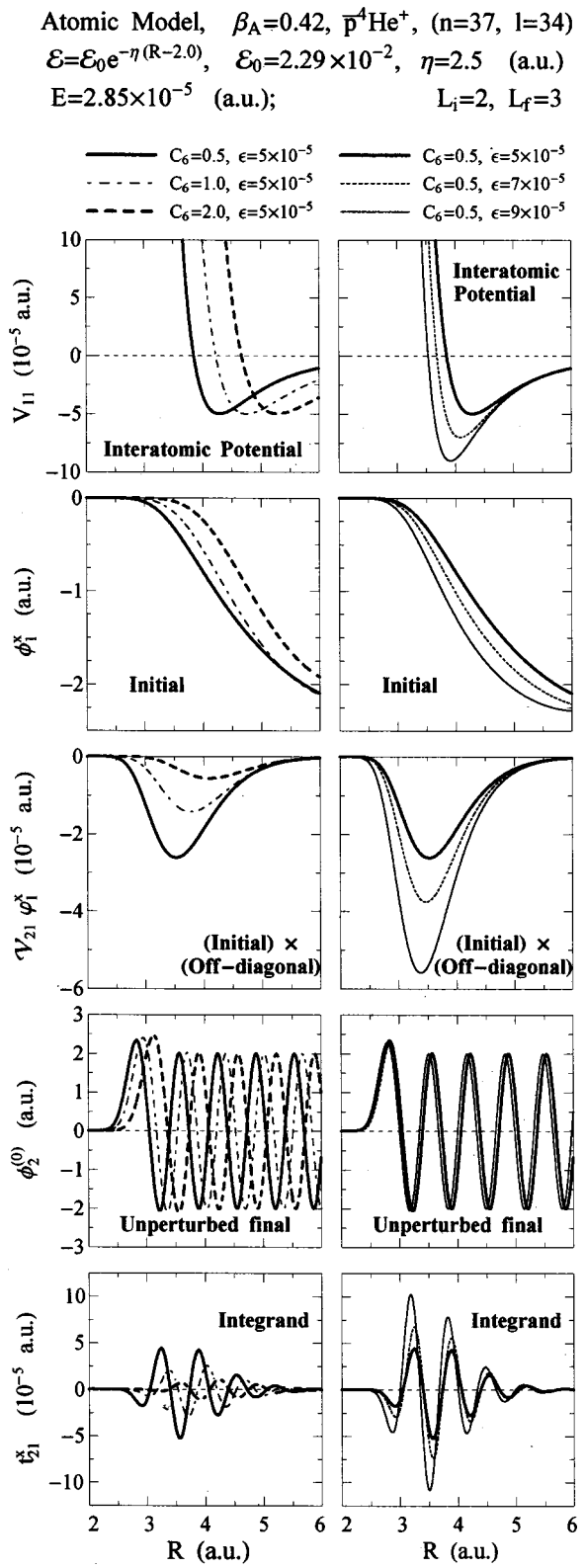

FIG. 6. V_{11}, ϕ_1^x, $\mathcal{V}_{21}\phi_1^x$, $\phi_2^{(0)}$, and $t_{21}^x=\phi_2^{(0)}\mathcal{V}_{21}\phi_1^x$ for five combinations of C_6 and ϵ, always with $V_{11}=V_{22}$.

ible with experiment. γ_S is much too low in every instance. The highest rate, computed with

$$C_6=1.0, \quad \epsilon=5\times10^{-5}, \quad \alpha=14.15, \tag{24}$$

is too low by a factor of ~45. The discrepancy for the seemingly realistic set in Eq. (23) is a factor of ~1300.

(c) C_6 outside its selected range. The failure to achieve agreement with experiment with any parameter set within the selected ranges is why estimates have been included with $C_6=0.5$. This leads to low R_m. The set

$$C_6=0.5, \quad \epsilon=9\times10^{-5}, \quad \alpha=17.0 \tag{25}$$

leads to $\gamma_S=1.05\times10^6$ s^{-1}, close to the required value. It could be argued that this might be acceptable, as there is no need for a potential with an accurate asymptotic form. But this conclusion requires a reason for discarding the seemingly realistic set in Eq. (23).

(d) Difficulty with R_m. Equations (23) and (25) lead to rather different potentials. Not only do their depths differ by a factor of 3, but R_m is only 3.91 for Eq. (25), as compared to 5.50 for Eq. (23). Because of results reported in Refs. [8,11,12], a value of R_m significantly less than 5 is difficult to accept while retaining the assumption that V_{11} and V_{22} depend only on n, l, and R. Before abandoning this assumption, we performed more computations. We allowed $\mathcal{E}$ to change. We also allowed the parameter sets for V_{11} and V_{22} to differ by reasonable amounts. As outlined in Secs. III B 2 and III C, there is little reason to believe that any rate obtained with parameters not too different from Eq. (23) could be in agreement with experiment.

2. Dependence on $\mathcal{E}(R)$

Though all γ_S in Figs. 2 and 3 were computed using the same $\mathcal{E}(R)$, we did investigate the consequences of using different $\mathcal{E}$. Because of results summarized below, we have concluded that agreement with experiment is unlikely to be achieved with any reasonable—and, in some instances, even a not very reasonable—change in $\mathcal{E}$ if our assumed parameter ranges for V_{11} and V_{22} are retained.

(a) Dependence on η. There is no crucial dependence of γ_S on η. For every combination of Exp-6 parameters used for Figs. 2 and 3, varying η by as much as 25% causes γ_S to change by no more than ~40%. In most instances the change is considerably less than 40%, and in no instance is there an increase of more than ~20%.

(b) Dependence on functional form. We were unable to detect any crucial dependence of γ_S on the functional form of $\mathcal{E}$. We recalculated all rates in Figs. 2 and 3 for $C_6\leqslant2.5$, but using instead $\mathcal{E}_{E6}$, as defined in Eq. (11), with the parameters in Eq. (12). Though the result was always larger, the increase was only between 30% and 80%. Also, we found that a change of as much as 75% in either $\epsilon^{(od)}$ or $C_6^{(od)}$ never causes γ_S to become more than approximately three times larger. We did find that an increase of as much as 25% in $\alpha^{(od)}$ causes γ_S to be larger by as much as a factor of ~35. This is still not large enough to achieve agreement with experiment.

(c) Assuming $\mathcal{E}=-\partial V_{11}/\partial R$. Our assumption of the adequacy of the estimates in Ref. [13] notwithstanding, we repeated the computation of γ_S for all combinations of C_6, ϵ, and α selected for Figs. 2 and 3, but using instead a field

of the form $\mathcal{E}_{E6}$, with the parameters for $\mathcal{V}_B$ in Eq. (11) being equated to those for the potential V_{11} used in Eq. (20). The results were in some cases considerably greater. But except for a few instances with $C_6=0.5$ or 1.0, γ_S still remained well below 0.7×10^6 s^{-1}. For the potential specified by Eq. (23), it remained too low by a factor of ~30.

(d) Breakdown of quadratic dependence on $f\beta_M\mathcal{E}_0$. The transition-inducing electric field must satisfy a fairly tight constraint if the calculation of γ_S is to remain relatively simple. We repeated the computations leading to many of the rates shown in Figs. 2 and 3, but using instead a wide variation of values of the product $f\beta_M\mathcal{E}_0$. This product was allowed to be as much as 14 times larger than 2.29×10^{-2}, the guessed value of $\mathcal{E}_0$ in Eq. (10). This gave rates that would be obtained with $\mathcal{E}_0$ being up to 23 times larger than in Eq. (10). These rates, which are all much below the required value, are well behaved only for the lower values of $f\beta_M\mathcal{E}_0$. Probably, this causes no significant inadequacy in our way of computing γ_S, because if $\mathcal{E}_0$ differs by no more than 75% from the estimate in Eq. (10), the dependence of γ_S on $f\beta_M\mathcal{E}_0$ remains more or less quadratic, in many instances almost precisely so. However, if $f\beta_M\mathcal{E}_0$ is larger than 2.29×10^{-2} by a factor as small as 2.0, the dependence on β_M for some parameter sets is no longer even approximately quadratic.

3. Comparison with atomic model

Rate calculations were performed with both models and a wide selection of the parameter combinations for V_{11} and V_{22} used for Figs. 2 and 3, though with $\mathcal{E}_0$ always being ten times smaller than in Eq. (10) so as to avoid any complication due to the dependence on $f\beta_A\mathcal{E}_0$ or $f\beta_M\mathcal{E}_0$ not being precisely quadratic. It was assumed that V_{11} and V_{22} in Eq. (20) are the same as in Eq. (3). The atomic model always gave a rate that was not much larger, the difference ranging from 6% to 19%. There are several reasons for this near agreement with our very approximate implementation of the molecular model. (i) Even though the two models use different Hamiltonians and, therefore, different representations, both use the same $\mathcal{E}$ and, in the present paper, nearly the same interatomic potentials. (ii) For all $L_i\geqslant1$, the appropriate sums and averages of β_A^2 and β_M^2 are precisely the same, while for $L_i=0$ they differ only by a factor of 5/3, the one for the atomic model being the larger. (iii) For the energies and splittings being considered here, the term $L_f(L_f+1)/(2\mu R^2)$ in the effective radial potential for the much more energetic final state should not be very important. (iv) In the limit of very large R, both models use essentially the same set of initial and final states of $\bar{p}\mathrm{He}^+$, the two sets differing only by rotations.

4. Dependence on ΔE

Figure 4 shows, for a parameter combination used for Figs. 2 and 3, estimates of γ_S if ΔE is varied by as much as 50% from its correct value. γ_S is very sensitive to ΔE. In Fig. 4, it spans five orders of magnitude. For the same $\mathcal{E}$, but for other parameter combinations spanning the ranges shown in Fig. 1, γ_S varies with ΔE in ways more or less similar to Fig. 4. The dependence of $\log\gamma_S$ on ΔE always remains nearly linear, though the difference between the minimum and maximum γ_S for 50% changes in ΔE varies between three and six orders of magnitude, usually becoming smaller as γ_S for the correct splitting becomes larger.

Stark rates in $\bar{p}\mathrm{He}^+$, though much lower than the radiative rate in most instances, should be much faster than in comparable states of $K^-\mathrm{He}^+$.

5. γ_S for $\bar{p}^3He^+$

The large variations of γ_S in Fig. 4 suggest an explanation of the large difference between the disappearance rates of the (36,33) state of $\bar{p}^3\mathrm{He}^+$ and the (37,34) state of $\bar{p}^4\mathrm{He}^+$. It is apparent in Eq. (22) that ϕ_1 and ϕ_2 depend on ΔE only when it is effectively multiplied by μ. A smaller μ should affect a rate in the same way as a smaller ΔE.

Figure 5 shows estimates of the ratio of γ_S for the (36,33) state of $\bar{p}^3\mathrm{He}^+$ to γ_S for the (37,34) state of $\bar{p}^4\mathrm{He}^+$. Many parameter sets for V_{11} and V_{22} were used, but for each ratio both rates were computed with the same set. The differences in γ_S for $\bar{p}^3\mathrm{He}^+$ and $\bar{p}^4\mathrm{He}^+$ are partly due to the relatively small difference in ΔE (3.6% higher for $\bar{p}^3\mathrm{He}^+$), but mostly due to the relatively large difference in μ (23% lower for $\bar{p}^3\mathrm{He}^+$-^{3}He). Some of these ratios are more than twice as large as the factor of ~10 reported in Ref. [4]. The difference in reduced mass seems likely to account for much, if not all, of the ^{3}He-^{4}He rate difference.

6. T matrix calculations with the atomic model

T matrix calculations shed a bit more light on the relationship between a cross section and the $\bar{p}\mathrm{He}^+$-He interaction. The relationship is not especially simple because ΔE is so large. The T matrix element can be written as

$$T_{21}=e^{i\xi}\int_0^\infty t_{21}(R)\,dR, \tag{26a}$$

$$t_{21}(R)=\phi_2^{(0)}(R)\mathcal{V}_{21}(R)[\phi_1^x(R)+i\phi_1^y(R)], \tag{26b}$$

$$\phi_1^x(R)=\mathrm{Re}[e^{-i\xi}\phi_1(R)], \tag{26c}$$

$$\phi_1^y(R)=\mathrm{Im}[e^{-i\xi}\phi_1(R)], \tag{26d}$$

$$e^{i\xi}=\phi_1(R_c)/|\phi_1(R_c)|, \tag{26e}$$

$$R_c=1000, \tag{26f}$$

where R_c is the large separation at which we ordinarily evaluated cross sections using probability currents, ϕ_1 is a component of the solution of Eq. (7) used to evaluate the currents, $\mathcal{V}_{21}$ is defined by Eq. (8), and $\phi_2^{(0)}$ is a component of a regular solution of Eq. (7) if $\mathcal{V}_{21}=0$.

If ϕ_1^y in Eq. (26b) is neglected, there is in almost every instance only negligible change in the computed cross section. A few results obtained with this approximation are presented in Fig. 6 and Table I. It was assumed in every instance that $E=2.85\times10^{-5}$, $L_i=2$, $L_f=3$, and $\beta_A=0.42$. It was also assumed that $\mathcal{E}$ is given by Eq. (9), with the parameters

TABLE I. Partial cross sections for a Stark transition from the (37,34) state of $\bar{p}^4He^+$, and the ratio of the integrals of $|t_{21}^x|$ and t_{21}^x. In each instance, $L_i=2$ and $L_f=3$.

C_6 (a.u.)	ϵ (a.u.)	α (a.u.)	$\sigma^T_{L_i\to L_f}$ (cm^2)	$\sigma^C_{L_i\to L_f}$ (cm^2)	$\left(\int_0^\infty \lvert t_{21}^x(R)\rvert dR\right) \Big/ \left(\int_0^\infty t_{21}^x(R)dR\right)$
2.0	5×10^{-5}	13.20	1.641×10^{-23}	1.644×10^{-23}	-224
1.0	5×10^{-5}	14.15	2.764×10^{-22}	2.770×10^{-22}	-131
0.5	5×10^{-5}	16.0	2.424×10^{-21}	2.429×10^{-21}	-77
0.5	7×10^{-5}	17.0	7.845×10^{-21}	7.861×10^{-21}	-59
0.5	9×10^{-5}	17.0	2.070×10^{-20}	2.075×10^{-20}	-52

in Eq. (10). Five combinations of C_6, ϵ, and α are listed, in every instance identical to a combination used for Figs. 2 and 3. Figure 6 shows V_{11}, ϕ_1^x, $\mathcal{V}_{21}\phi_1^x$, $\phi_2^{(0)}$, and $t_{21}^x = \phi_2^{(0)}\mathcal{V}_{21}\phi_1^x$. Both of the real functions ϕ_1^x and $\phi_2^{(0)}$ are normalized so as to be decomposable into superpositions of ingoing and outgoing waves with amplitudes of magnitude 1.0. Table I lists the partial cross section $\sigma^T_{L_i\to L_f}$ computed with the T matrix, the partial cross section $\sigma^C_{L_i\to L_f}$ computed with probability currents, and the ratio of the integrals of $|t_{21}^x|$ and t_{21}^x. There is, with appreciable variation, much cancellation of the contributions of t_{21}^x to T_{21}.

It seems clear from Figs. 3 and 6, and from Table I, that there is increased overlap between the initial and final wave functions—and a much increased Stark rate—if R_m is rather low. This can be achieved by using a low value of C_6. The overlap can also be increased by increasing ϵ.

7. Effect of possible shape resonances

Computations of γ_S were examined for a wide selection of instances where shape resonances might be important. No significant effect was found. Such resonances do indeed occur, and they give rise to dramatic increases in partial cross sections. But no resonance contributed significantly to a thermally averaged rate.

C. Molecular model with $V_{11}\neq V_{22}$

We first note that allowing α to be two or three units higher for V_{22} than for V_{11} can result in a very large γ_S, in some instances enormously larger than in Figs. 2 and 3. In such cases, V_{11} and $V_{22}-\Delta E$ become equal at a separation greater than both classical turning points, and there is a high probability of a Landau-Zener transition. We believe this does not happen. Figure 1 suggests that differences in α for neighboring states should be smaller than 1.0, probably much smaller. As shown below, such differences should not result in γ_S being changed by more than an order of magnitude.

We investigated the effects of reasonable variations of V_{22} from V_{11}, the latter being specified in turn by Eqs. (4) and (23). We required the difference between V_{11} and V_{22} to be, in our judgment, less than the difference between potentials for nearby states with nearly the same l but a one-unit difference in n. This is not a stringent requirement, as energy differences between such states are an order of magnitude greater than those between states with the same n but a one-unit difference in l.

There are not many estimates of V_{11} and V_{22} for states of exotic helium with a one-unit difference in n and nearly the same l. A few of these are in Ref. [13] and are for circular orbits of K^-He^+ with $n=27$, 28, and 29. Another is in Ref. [8] and is for $\bar{p}^4He^+$ with $n=38$ and 39. We used the potentials in Ref. [8]—and we took into account the ranges of α in Fig. 1 and the effect of introducing small changes in α for the potential specified by Eq. (4)—to devise four *ad hoc* conditions that we believe should be well satisfied by V_{11} and V_{22} for states with the same n but a one-unit difference in l. (i) They must become equal to 0 at separations differing by no more than 0.15. (ii) Their minima must occur at separations differing by no more than 0.15. (iii) Their minimum values must differ by no more than 10%. (iv) Their values of α must differ by no more than 1.0.

For a given V_{11}, each of the parameters for V_{22} was, in turn, varied to the largest extent possible without violating conditions (i)–(iv). In no instance was γ_S increased by more than a factor of 17. We conclude that the approximation $V_{11}=V_{22}$ is acceptable for our purposes.

IV. SUMMARY AND CONCLUSIONS

Estimates of thermally averaged Stark rates in Secs. III B 1, III B 3, and III C indicate that transitions are unlikely in metastable $\bar{p}^4He^+$ with $36\lesssim n\lesssim 38$ if the interatomic potentials depend only on n, l, and R. In particular, there is a large discrepancy—at least two orders of magnitude—between the observed quenching rate of the (37,34) state and estimates obtained with reasonable approximations to what is, to date, the best calculation of a (n,l)-dependent potential. To get rid of this discrepancy without introducing very different potentials would require increasing the guessed value of the transition-inducing electric field by what we believe would be too large an amount, at least an order of magnitude.

It is evident in Figs. 2, 3, and 6 that γ_S is very sensitive to the interatomic potential for the initial state. If this potential has a minimum, preferably relatively deep, at a separation rather smaller than can reasonably be expected if the dependence is only on n, l, and R, Stark transitions can be competitive with radiation.

We conjecture that the appropriate potentials for Stark transitions depend on the component m of $\bar{p}$ and electronic

orbital angular momentum along the momentary direction of the interatomic axis. In view of the relative speeds of the thermal atomic motion, the $\overline{p}$, and the electrons—and also in view of the $(\mathbf{R},\mathbf{r})$-dependent potential in Ref. [8], which has at points near $R=4.0$ and $\mathbf{R}\cdot\mathbf{r}=0$ a depth exceeding the thermal energy of the colliding atoms—this is, by itself, not a daring conjecture. We further conjecture that, for just a few combinations of n and l, potentials for just a few fairly large values of $|m|$ lead to Stark rates at $N=10^{21}$ cm^{-3} that are considerably in excess of the radiative rate and that contribute disproportionately to the quenching rate. The m dependence of such potentials would be largely a consequence of the distortion of the electronic motion, which should vary almost adiabatically with the position of the $\overline{p}$. As noted in Sec. II B 3, the potential seems likely to be deepest if $|m|=l$, though an angular factor complicates matters by causing Stark transitions to be unlikely unless $|m|$ is somewhat less than l. Our conjecture probably requires an appreciable l dependence of the well depth. If accurate estimates of Stark rates are ever to be obtained, improved calculations of the $\overline{p}$He$^+$-He interaction, taking into account the orientation of $\overline{p}$He$^+$, perhaps even taking into account the sort of configuration mixing that Kartavtsev *et al.* have suggested is important in some Auger transitions [21], appear to be needed.

Calculations presented in Sec. III B 6 suggest that much, if not all, of the difference between the Stark rates for the (36,33) state of $\overline{p}^3$He$^+$ and the (37,34) state of $\overline{p}^4$He$^+$ is due to the difference in reduced mass of the colliding atoms.

ACKNOWLEDGMENT

We thank F. C. Zhang for a helpful conversation.

[1] G.T. Condo, Phys. Lett. **9**, 65 (1964).
[2] J.E. Russell, Phys. Rev. Lett. **23**, 63 (1969).
[3] M. Hori *et al.*, Phys. Rev. A **58**, 1612 (1998).
[4] F.J. Hartmann *et al.*, Phys. Rev. A **58**, 3604 (1998).
[5] See, for example, R. Pohl *et al.*, Phys. Rev. A **58**, 4406 (1998), and references therein.
[6] E. Widmann *et al.*, Phys. Rev. A **51**, 2870 (1995).
[7] G.Ya. Korenman, Hyperfine Interact. **101/102**, 463 (1996).
[8] D. Bakalov *et al.*, Phys. Rev. Lett. **84**, 2350 (2000).
[9] V.I. Korobov and D.D. Bakalov, Phys. Rev. Lett. **79**, 3379 (1997).
[10] T.B. Day, G.A. Snow, and J. Sucher, Phys. Rev. Lett. **3**, 61 (1959).
[11] J.P. Toennies, W. Welz, and G. Wolf, J. Chem. Phys. **71**, 614 (1979).
[12] J.P. Toennies, W. Welz, and G. Wolf, Chem. Phys. Lett. **44**, 5 (1976).
[13] J.E. Russell, Phys. Rev. **188**, 187 (1969).
[14] Y.M. Chan and A. Dalgarno, Proc. Phys. Soc. London **86**, 777 (1965).
[15] J.E. Russell, Phys. Rev. A **1**, 735 (1970).
[16] T. Yamazaki and K. Ohtsuki, Phys. Rev. A **45**, 7782 (1992).
[17] I. Shimamura, Phys. Rev. A **46**, 3776 (1992).
[18] B. Zygelman, Phys. Lett. A **125**, 476 (1987).
[19] J. Moody, A. Shapere, and F. Wilczek, in *Geometric Phases in Physics*, edited by A. Shapere and F. Wilczek, Advanced Series in Mathematical Physics Vol. 5 (World Scientific, Singapore, 1989), p. 160.
[20] O.I. Kartavtsev, Yad. Fiz. **59**, 1541 (1996) [Phys. At. Nucl. **59**, 1483 (1996)].
[21] O.I. Kartavtsev, D.E. Monakhov, and S.I. Fedotov, Phys. Rev. A **61**, 062507 (2000); **63**, 019901(E) (2001).